Mat. Res. Soc. Symp. Proc. Vol. 746 © 2003 Materials Research Society Q1.3

Defects, Tunneling, and EPR Spectra of Single-Molecule Magnets

Kyungwha Park[1,2,3], M. A. Novotny[4], N. S. Dalal[3], S. Hill[5], P. A. Rikvold[1,6], S. Bhaduri[7], G. Christou[7], and D. N. Hendrickson[8]
[1]School of Computational Science and Information Technology, Florida State University, Tallahassee, Florida 32306
[2]Department of Chemistry and Biochemistry, Florida State University, Tallahassee, Florida 32306
[3] Center for Computational Materials Science, Code 6390, Naval Research Laboratory, Washington DC 20375
[4]Department of Physics and Astronomy and the Engineering Research Center, Mississippi State University, Mississippi State, Mississippi 39762
[5]Department of Physics, University of Florida, Gainesville, Florida 32611
[6]Center for Materials Research and Technology and Department of Physics, Florida State University, Tallahassee, Florida 32306
[7]Department of Chemistry, University of Florida, Gainesville, Florida 32611
[8]Department of Chemistry and Biochemistry, University of California at San Diego, La Jolla, California 92093

ABSTRACT

We examine theoretically electron paramagnetic resonance (EPR) lineshapes as functions of resonance frequency, energy level, and temperature for single crystals of three different kinds of single-molecule nanomagnets (SMMs): Mn_{12} acetate, Fe_8Br, and the $S = 9/2$ Mn_4 compound. We use a density-matrix equation and consider distributions in the uniaxial (second-order) anisotropy parameter D and the g factor, caused by possible defects in the samples. Additionally, weak intermolecular exchange and electronic dipole interactions are included in a mean-field approximation. Our calculated linewidths are in good agreement with experiments. We find that the distribution in D is common to the three examined single-molecule magnets. This could provide a basis for a proposed tunneling mechanism due to lattice defects or imperfections. We also find that weak intermolecular exchange and dipolar interactions are mainly responsible for the temperature dependence of the lineshapes for all three SMMs, and that the intermolecular exchange interaction is more significant for Mn_4 than for the other two SMMs. This finding is consistent with earlier experiments and suggests the role of spin-spin relaxation processes in the mechanism of magnetization tunneling.

INTRODUCTION

Single-molecule magnets (SMMs) have recently been the focus of much attention because of the possibility of macroscopic quantum tunneling of their magnetizations [1, 2] and possible applications in magnetic storage devices and quantum computers

[3]. SMMs are composed of identical single-domain nanoscale molecules, comprised of a core of several transition-metal ions surrounded by many different species of atoms, and they have a large effective spin. The characteristics of SMMs are relatively weak exchange and dipolar interactions between molecules, a large zero-field energy barrier against magnetization reversal, and magnetization steps in their hysteresis loops, which indicate quantum tunneling despite the large spin values [4, 5, 6, 7, 8].

In this paper, we examine three different molecular magnets, which are briefly described in the following. The most extensively studied single-molecule magnet is $[Mn_{12}O_{12}(CH_3COO)_{16}(H_2O_4)]\cdot 2CH_3COOH\cdot 4H_2O$ (abbreviated hereafter as Mn_{12}), which was first synthesized by Lis [9]. Each molecule in Mn_{12} has an effective spin of $S = 10$. It is a uniaxial system with a zero-field energy barrier against magnetization reversal of 65 K [5, 6, 7]. Another well-studied magnet is $[Fe_8O_2(OH)_{12}(tacn)_6]Br_8\cdot 9H_2O$ (abbreviated as Fe_8) [10]. Each molecule in Fe_8 also has a spin of $S = 10$ with a magnetization-reversal barrier of 30 K [11, 12]. This is a biaxial system so exhibits oscillations in tunneling rates with transverse magnetic field [13]. Recently synthesized is $[Mn_4O_3(OSiMe)_3(O_2CEt)_3(dbm)_3]$ (abbreviated as Mn_4). Each molecule in Mn_4 consists of two kinds of Mn ions with mixed valence: three Mn^{3+} ($S = 2$) and one Mn^{4+} ($S = 3/2$) are located in a distorted cubane structure and antiferromagnetically coupled to give a ground-state spin of $S = 9/2$. The approximate magnetization-reversal energy barrier is 13 K in zero field [14]. All three of these SMMs show clear magnetization steps in hysteresis loops below their blocking temperatures.

Recently, electron paramagnetic resonance (EPR) experiments [12, 14, 15, 16] on single crystals of these SMMs showed interesting results for the lineshapes as a function of EPR resonance frequency, energy levels involved in the EPR transitions, and temperature. The temperatures employed are in the 2–50 K range, and the frequencies are in the 40–190 GHz range. We focus on the case when the magnetic field is applied along the easy axis at fixed frequency. In this case, the measured linewidths are much broader than the homogeneous line broadening caused by the lifetimes of the energy levels, and the linewidths increase as lower energy levels are involved with the EPR transitions. Additionally, some interesting features have been observed in the temperature dependence of the linewidths and lineshapes of the EPR spectra [6, 12, 14, 15, 16]. These temperature dependences were different for different molecular magnets. In this paper, we summarize our theoretical understanding of the linewidths' dependence on frequency, energy level, and temperature for the three molecular magnets, Mn_{12}, Fe_8, and Mn_4. We also provide quantitative comparison of our calculated results with experimental data. The theoretical results on Mn_4 are preliminary and work on this system is still in progress.

MODEL

We start with a single-spin effective Hamiltonian considering embedded symmetry in each molecule and calculate the resonance linewidths using a density-matrix equation [17]. We find that an entirely single-spin picture cannot explain even qualitative trends in

the experimental data. Thus, it is inevitable to include many-body effects. As a simple start, we assume that the second-order uniaxial anisotropy parameter, D, and the g factor may not be the same for all molecules. The microscopic origin of the distribution in D has not yet been fully understood [18, 19]. In addition, each molecule may interact with the rest of the molecules through exchange and/or dipolar interactions. Details of the model and the technique are discussed in Refs. [15, 20, 21, 22]. This section is based in part on our earlier work [15, 20].

Since each molecule in Mn_{12} has approximate S_4 symmetry, the dominant single-spin Hamiltonian reads, with applied magnetic field along the easy magnetization axis (z axis),

$$\mathcal{H}_0 = -DS_z^2 - CS_z^4 - g\mu_B HS_z \,, \tag{1}$$

where $D = 0.55$ K; $C = 1.17 \times 10^{-3}$ K, and $g = 1.94$ [5]. The SMM Fe_8 has approximate D_2 symmetry, so the Hamiltonian reads

$$\mathcal{H}_0 = -DS_z^2 - E(S_x^2 - S_y^2) - g\mu_B HS_z \,, \tag{2}$$

where $D = 0.288$ K, $E = 0.043$ K, and $g = 2.0$ [12]. In our calculations for Fe_8, we neglect the small E term because we are interested in the case with the applied field along the easy axis. The SMM Mn_4 has C_3 symmetry, so the Hamiltonian reads

$$\mathcal{H}_0 = -DS_z^2 - CS_z^4 - g\mu_B HS_z \,, \tag{3}$$

where $D = 0.632$ K, $C = 3.12 \times 10^{-3}$ K, and $g = 2.0$ [14].

We now introduce an interaction $V(t)$ between the spin system and an oscillating transverse magnetic field H_x with angular frequency $\omega \equiv 2\pi\nu$. The interaction of the spin system with the environment is governed by a time dependent density-matrix equation [17, 23]. The power absorption between the energy levels M_s and $M_s - 1$ from the oscillating field, up to first order in V_0 and near resonance (with a fixed value of D), is written as

$$\frac{\mathrm{d}\mathcal{E}}{\mathrm{d}t} = \frac{(\mathcal{E}_{M_s-1} - \mathcal{E}_{M_s})}{\hbar^2} |\langle M_s|V_0|M_s - 1\rangle|^2 \Delta(H)(\rho_{M_s} - \rho_{M_s-1}) \,, \tag{4}$$

$$\Delta(H) \equiv \frac{\hbar^2 \gamma_{M_s-1,M_s}}{(g\mu_B)^2(H - H_{\rm res})^2 + (\hbar\gamma_{M_s-1,M_s})^2} \,, \tag{5}$$

$$H_{\rm res} \equiv \frac{\hbar\omega - D(2M_s - 1) - C(4M_s^3 - 6M_s^2 + 4M_s - 1)}{g\mu_B} \,, \tag{6}$$

where V_0 is the strength of the interaction $V(t)$, $\mathcal{E}_{M_s}$ is the energy of the level M_s, ρ_{M_s} is the population of the level M_s, $\Delta(H)$ is a Lorentzian lineshape function, and $H_{\rm res}$ is the resonance field for Mn_{12} and Mn_4. (For Fe_8 there is no C term.) The ratio $\hbar\gamma_{M_s-1,M_s}/g\mu_B$ gives a linewidth due to the finite lifetime of any excited state. The linewidths determined by γ_{M_s-1,M_s} are on the order of several to several tens of gauss at the measured temperature (10 K for Fe_8 and Mn_4 and 25 K for Mn_{12}), and they

decrease with increasing M_s. (In our convention, $M_s = +10$ is the ground state with $H > 0$.) However, the measured linewidths *increase* with increasing M_s, and the order of magnitude of the widths is a couple of hundred to a thousand gauss. Additionally, the dramatic temperature dependence of the linewidths cannot be explained by homogeneous broadening alone.

To resolve this discrepancy, we include distributions in D and g, (called D-strain and g-strain effects, respectively) and intermolecular exchange and dipolar interactions. With Gaussian distributions in D and g, centered at the experimentally determined values and with small standard deviations σ_D and σ_g, we can average the power absorption (equation 4) over the distributions. To calculate the effect on the linewidths of the intermolecular exchange and dipolar interactions with fixed D and g, we use a multispin Hamiltonian [20, 21, 22]:

$$\mathcal{H}^{\text{tot}} = \sum_i [\,\mathcal{H}_{0i} + V_i(t)\,] + \mathcal{H}^{(1)}\,, \quad \mathcal{H}^{(1)} \equiv \mathcal{H}^{\text{dipole}} + \mathcal{H}^{\text{exch}}\,, \tag{7}$$

$$\mathcal{H}^{\text{dipole}} = \frac{1}{2}{\sum_{jk}}' A_{jk}(\vec{S}_j \cdot \vec{S}_k - 3S_j^z S_k^z)\,, \tag{8}$$

$$A_{jk} \equiv \left(\frac{\mu_0}{4\pi}\right)\frac{(g\mu_B)^2}{2r_{jk}^3}(3\zeta_{jk}^2 - 1)\,, \tag{9}$$

$$\mathcal{H}^{\text{exch}} = \frac{1}{2}{\sum_{jk}}' J_{jk}\,\vec{S}_j \cdot \vec{S}_k\,, \tag{10}$$

where $\mathcal{H}_{0i}$ is the single-spin Hamiltonian for the ith molecule, the sum $\sum_i$ runs over all molecules, and $V_i(t)$ is the interaction between the ith molecule and the oscillating transverse field. Here $\mathcal{H}^{\text{dipole}}$ is the dipolar interaction between the molecules, and ζ_{jk} are the direction cosines of the vector between molecules j and k ($\vec{r}_{jk}$) relative to the easy axis (z axis). The sum $\sum'_{jk}$ runs over all molecules, so that any two indices are not the same. $\mathcal{H}^{\text{exch}}$ is the isotropic exchange interaction between the spins of nearest-neighbor molecules, where the exchange coupling constant J_{ij} is J if the ith and jth spins are nearest neighbors and zero otherwise. Assuming that $\sum_i V_i(t)$ is much smaller than $\mathcal{H}^{(1)}$, which again is much smaller than $\sum_i \mathcal{H}_{0i}$, we neglect $\sum_i V_i(t)$ and treat $\mathcal{H}^{(1)}$ perturbatively. In a mean-field approximation, the sums of A_{jk} and J_{jk} (equations 9 and 10) can be separated from the spin operators.

Using the multispin Hamiltonian, we construct a probability density function for the resonance field. To compare with the measured linewidths, we calculate the second central moment of the resonance field, $\langle (H - \langle H \rangle)^2 \rangle$, to zero order in $\mathcal{H}^{(1)}/k_BT$. To explain the experimental data, we need to vary two parameters for the D-strain and g-strain effects, and to vary three parameters [20] for the contribution of the spin-spin interactions: $\sum'_{ij} J_{ij}^2$, $\Gamma \equiv \sum'_{ij} A_{ij}^2$, and $\Lambda \equiv \sum'_{ij} J_{ij} A_{ij}$.

RESULTS AND DISCUSSION

We find that the uniaxial anisotropy parameter D is randomly distributed in all

three of the molecular magnets. This may be due to possible defects or imperfections in the the samples. For Mn_{12} and Mn_4, the distribution in the g factor is also important, although this effect is not significant for Fe_8. The spreads in D and g vary from sample to sample by 30−40%. The effect of the distribution in D on inhomogeneous broadening was observed in terahertz spectroscopy for Mn_{12} [24]. The temperature dependence of the linewidths is mainly caused by the spin-spin interactions. The dipolar field was measured in a millimeter-wave study of Fe_8 [25]. For Mn_4, the intermolecular exchange interaction is stronger than the dipolar interaction, which is consistent with experiments on Mn_4 dimers [26] and monomers [27, 28]. For clarity, we discuss each SMM separately.

Fe_8

We find that for Fe_8 the distribution in D and the intermolecular exchange and dipolar interactions contribute to the linewidths. The distribution in D makes the linewidth increase with increasing energy level M_s, which can be seen from the resonance-field expression (equation 6). The intermolecular exchange and dipolar interactions make the linewidths increase with increasing M_s and with decreasing the resonance frequency ν. The reason is that the resonance field decreases with increasing M_s and with decreasing ν, which can be understood by equation 6. Combining the effect of the distribution in D with the exchange and dipolar interactions explains well the trend and the magnitude of the measured linewidths as functions of frequency and energy level [15].

Next we discuss the temperature dependence of the linewdiths. The distribution in D alone cannot explain the interesting measured temperature dependence of the linewidths shown as symbols in figure 1 (a). The reason is that the linewidths caused by the distribution in D are only slightly temperature dependent due to the temperature dependence of the natural linewidths $\hbar\gamma_{M_s-1,M_s}/g\mu_B$ in equation 5. So this weak temperature dependence is monotonic and noticeable only for the small M_s (at most about 100 G at 30 K for $M_s = 3$) [20]. However, the linewidths caused solely by the exchange and dipolar interactions at fixed D and g vary significantly with temperature, as shown in figure 1 (b). For the ground state $M_s = 10$, the linewidths decrease with increasing temperature in the whole temperature range. For $M_s = 9$, 8, and 7, the widths first increase sharply with temperature at low temperatures, and then decrease slowly with temperature at high temperatures. For $M_s = 6$, 5, 4, and 3, the widths increase with increasing temperature in the whole range. This trend was also seen in the experimental linewidths, confirming that the exchange and dipolar interactions are crucial to understanding the temperature dependence of the linewidths. The calculated linewidths including the distribution in D and the spin-spin interactions are shown as curves in figure 1 (a). Here we use $\sigma_D \sim 0.0064\ D$, $J = -7$ G, $\Gamma = 86$ G^2, and $\Lambda = -156$ G^2. The calculated linewidths agree with the measured linewidths except in the low-temperature range for large M_s transitions ($M_s = 10, 9, 8$). At present, we do not fully understand this discrepancy. We note that the quality of the fit that includes a small ferromagnetic exchange interaction is comparable with that without exchange interaction, because the exchange coupling constant is small compared with the linewidths[29].

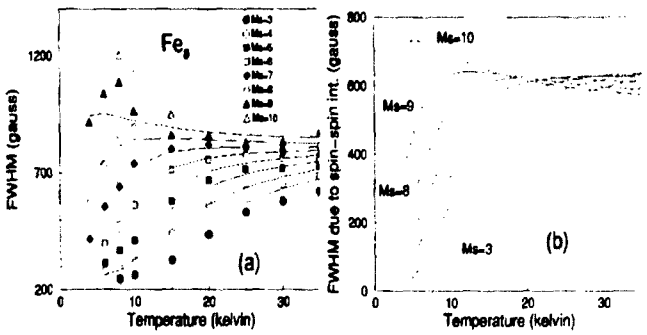

Figure 1: (a) Calculated (curves) and measured (symbols) FWHM vs temperature at $\nu = 116.9$ GHz for Fe_8. Here the standard deviation of D, $\sigma_D \sim 0.0064D$, the exchange constant $J = -7$ G, $\Gamma = \sum'_{ij} A_{ij}^2/N = 86$ G^2, and $\Lambda = \sum'_{ij} J_{ij} A_{ij}/N = -156$ G^2. The solid curves, from bottom to top, correspond to $M_s = 3, 4, ..., 9, 10$. (b) Calculated FWHM caused by the exchange and dipolar interactions only, shown vs temperature at $\nu = 116$ GHz for Fe_8. Here $J = -7$ G, $\Gamma = 86$ G^2, and $\Lambda = -156$ G^2. Cited from Ref. [20].

Mn_{12}

We find that the inhomogeneous line broadening for Mn_{12} is due to the distributions in D and g, and to the dipolar interactions. The distribution in D contributes to the variation of the linewidth as a function of M_s and ν in the same way as for Fe_8. The distribution in g makes the linewidths *decrease* with increasing M_s and decreasing ν, which is opposite to the effect of the distribution in D. The reason is that the resonance field decreases with increasing M_s and decreasing ν. The temperature dependence of the linewidths caused by only the distributions in D and g is very weak, so that it cannot explain the measured linewidths shown as symbols in figure 2 (a), which is similar to those for Fe_8. The contribution of the dipolar interactions to the linewidths is shown as a function of temperature in figure 2 (b). Unlike for Fe_8, the M_s dependence of the dipolar broadening does not decrease with increasing temperature (the curves are almost parallel as the temperature increases). Combining the three effects (distributions in D and g, and dipolar interactions), we find that the calculated linewidths agree well with the experimental data with $\sigma_D \sim 0.018D$, $\sigma_g \sim 0.002g$, and $\Gamma = 203$ G^2, as shown in figure 2 (a). Compared to the linewidths for Fe_8, the relatively weak temperature dependence for Mn_{12} indicates that for Mn_{12} the dipolar broadening is overshadowed

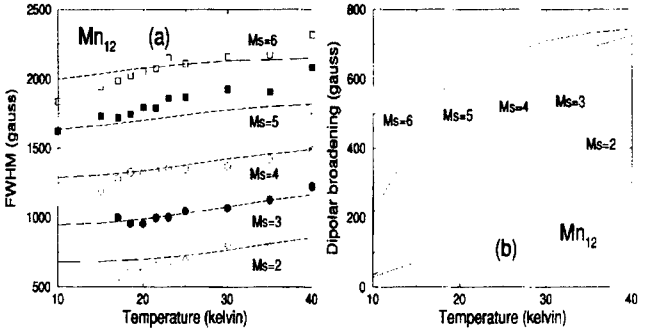

Figure 2: (a) Calculated (curves) and measured (symbols) FWHM vs temperature at $\nu = 189.123$ GHz for Mn_{12}. Here the D strain ($\sigma_D \sim 0.018D$), g strain ($\sigma_g \sim 0.002g$), and the dipolar interactions ($\Gamma = 203$ G^2) are included in the calculated linewidths. (b) Calculated FWHM caused by the dipolar interactions only, shown vs temperature, at $\nu = 189.123$ GHz with $\Gamma = 203$ G^2 for Mn_{12}. The examined temperature range for Mn_{12} is from 10 K to 40 K. Cited from Ref.[20].

by the effect of the distribution in D, which is three times as wide as for Fe_8. With the same parameter values, we also check that the M_s and frequency dependence of the measured linewidths can be explained.

Mn_4

We find that for Mn_4 all of our considerations of the many-body effects - the distributions in D and g, and the intermolecular exchange and dipolar interactions - substantially affect the inhomogeneous broadening. One minor difference of this SMM from the other two SMMs is that the effect of the distribution in D disappears in the transition $M_s = 1/2 \rightarrow -1/2$ because the resonance field (equation 6) does not depend on D at this transition. To examine the temperature dependence of the linewidths caused solely by D-strain and g-strain, we used the same spin-phonon coupling parameters as for Mn_{12}[23] to obtain the order of magnitude of the lifetimes of the energy levels. As expected from the analysis of the two other SMMs, we also find that for Mn_4 the distributions in D and g do not significantly change the dependence of the linewidths on temperature.

Figure 3 (a) shows the calculated linewidths caused by the exchange and dipolar interactions only at fixed D and g versus temperature at $\nu = 138$ GHz. Here we use the exchange coupling constant $J = -40$ G, two nearest neighbors along the easy axis (because the nearest-neighbor distance along this direction is half of the nearest-

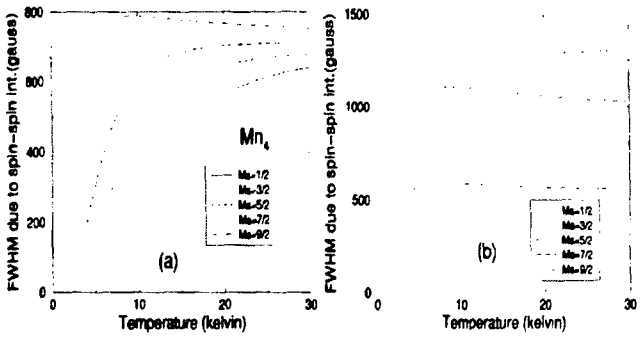

Figure 3: (a) Calculated linewidths due to the exchange and dipolar interactions only vs temperature at $\nu = 138$ GHz for Mn_4. Here we use the exchange coupling constant $J = -40$ G, $\Lambda = \sum'_{ij} J_{ij}A_{ij}/N = -1854.8$ G^2, and $\Gamma = \sum'_{ij} A^2_{ij}/N = 344$ G^2. (b) The same linewidths as in (a) when the sign of J is flipped and the other parameter values are kept the same.

neighbor distance perpendicular to this direction), $\Lambda = \sum'_{ij} J_{ij}A_{ij}/N = -1854.8$ G^2, and $\Gamma = \sum'_{ij} A^2_{ij}/N = 344$ G^2. The negative sign in J means ferromagnetically coupled spins. If we assume the approximate lattice geometry as a tetragonal lattice and take the easy axis as the crystal c axis, then we know that the sign of Λ should be the same as that of J. We explore some other possibilities of combining the exchange with the dipolar interaction. For example, figure 3 (b) shows the linewidths due to positive J (antiferromagnetically coupled) and the dipolar interaction. With positive J, the linewidth for $M_s = 9/2$ is greatly reduced and the linewidth for $M_s = 1/2$ is appreciably enhanced. This feature is quite different from the broadening with negative J.

Figure 4 shows the calculated linewidths versus temperature at $\nu = 138$ GHz. Here we use $\sigma_D = 0.01D$, $\sigma_g = 0.004g$, $J = -40$ G, $\Lambda = -1854.8$ G^2, and $\Gamma = 344$ G^2. The calculated linewidths agree reasonably with the experimental data except for the transition $M_s = 1/2 \rightarrow -1/2$. Notice that the magnitudes of the values of J and Λ are greatly enhanced compared to those for Fe_8. This suggests that Mn_4 has a stronger exchange interaction between molecules than Fe_8. Our value for J is different by a factor of 2 from the experimentally extracted value, $J = -74$ G [27]. Therefore, our finding may support the proposed mechanism of spin-spin cross relaxation in Mn_4 [27].

With the same parameter values, we can explain the frequency dependence of the linewidths at $T = 10$ K shown in figure 5. Although there are substantial distributions in D and g, the widths are somewhat dependent on the frequency, which indicates that the spin-spin interactions are not completely overshadowed by the D-strain and g-strain effects as in Mn_{12}. But definitely the frequency dependence is stronger than for Mn_{12} but weaker than for Fe_8.

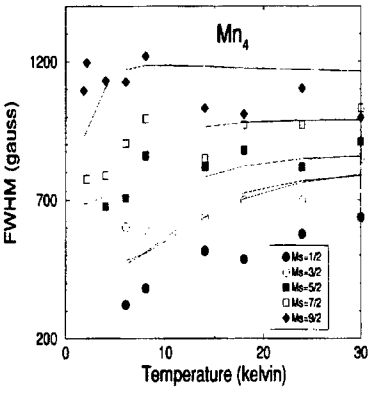

Figure 4: Calculated (curves) and measured (symbols) FWHM vs temperature at $\nu = 138$ GHz for Mn_4. Here we use $\sigma_D = 0.01D$, $\sigma_g = 0.004g$, $J = -40$ G, $\Lambda = \sum'_{ij} J_{ij}A_{ij}/N = -1854.8$ G^2, and $\Gamma = \sum'_{ij} A^2_{ij}/N = 344$ G^2. The solid curves, from bottom to top, correspond to $M_s = 1/2, 3/2, ..., 9/2$.

CONCLUSIONS

We investigated the EPR lineshapes as functions of resonance frequency ν, energy level M_s, and temperature T for the three different molecular magnets, Mn_{12}, Fe_8, and Mn_4, when the magnetic field is applied along the easy axis and the frequency is kept fixed. In our calculations, intermolecular exchange and dipolar interactions were included, as well as distributions in the uniaxial anisotropy parameter D and the g factor. We find that the distribution in D is present in all three SMMs but that the effect is strongest in Mn_{12}, and that the distribution in g contributes to the linewidths for Mn_{12} and Mn_4. The spin-spin interactions are responsible for the interesting trend of the temperature dependent lineshapes for all three magnets. For Mn_4, the exchange interaction is stronger than the dipolar interaction, which supports the conclusions derived from the earlier measurements[27]. The linewidths for the three magnets reveal different M_s, ν, and T dependences because of different contributions from the effects we are considering. Observation of EPR lineshapes could indicate which effects are dominant in a particular SMM, so that we may identify which mechanism leads to quantum tunneling.

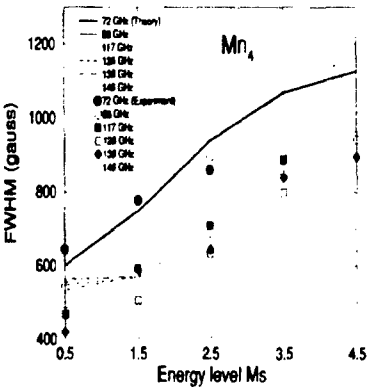

Figure 5: Calculated (curves) and measured (symbols) FWHM vs energy level M_s at $T = 10$ K for $\nu = 72$, 88, 117, 126, 138, and 146 GHz for Mn_4. Here the values of σ_D, σ_g, J, Γ, and Λ are the same as those in figure 4.

ACKNOWLEDGMENTS

This work was funded by NSF Grant Nos. DMR-9871455, DMR-0120310, DMR-0103290, and DMR-0196430, Research Corporation (S.H.), and by Florida State University through the School of Computational Science and Information Technology and the Center for Materials Research and Technology.

REFERENCES

1. *Quantum Tunneling of Magnetization - QTM '94*, Vol. 301 of *NATO Advanced Study Institute, Series E: Applied Sciences*, edited by L. Gunther and B. Barbara (Kluwer, Dordrecht, 1995).

2. E. M. Chudnovsky and J. Tejada, *Macroscopic Quantum Tunneling of the Magnetic Moment*, Cambridge Studies in Magnetism, Vol. 4 (Cambridge University Press, Cambridge, 1998) and references therein.

3. M. N. Leuenberger and D. Loss, Nature (London) **410**, 789 (2001).

4. J. Villain, F. Hartman-Boutron, R. Sessoli, and A. Rettori, Europhys. Lett. **27**, 159 (1994).

5. A. L. Barra, D. Gatteschi, and R. Sessoli, Phys. Rev. B **56**, 8192 (1997).

6. S. Hill, J. A. A. J. Perenboom, N. S. Dalal, T. Hathaway, T. Stalcup, and J. S. Brooks, Phys. Rev. Lett. **80**, 2453 (1998).

7. J. A. A. J. Perenboom, J. S. Brooks, S. Hill, T. Hathaway, and N. S. Dalal, Phys. Rev. B **58**, 330 (1998).

8. I. Mirebeau, M. Hennion, H. Casalta, H. Andres, H. U. Güdel, A. V. Irodova, and A. Caneschi, Phys. Rev. Lett. **83**, 628 (1999).

9. T. Lis, Acta Crystallogr. B **36**, 2042 (1980).

10. K. Wieghart, K. Pohl, I. Jibril, and G. Huttner, Angew. Chem. Int. Ed. Engl. **23**, 77 (1984).

11. E. del Barco, J. M. Hernandez, J. Tejada, N. Bisksup, R. Achey, I. Rutel, N. Dalal, and J. Brooks, Phys. Rev. B **62**, 3018 (2000).

12. S. Maccagnano, R. Achey, E. Negusse, A. Lussier, M. M. Mola, S. Hill, and N. S. Dalal, Polyhedron **20**, 1441 (2001).

13. A. Garg, Europhys. Lett. **22**, 205 (1993).

14. R. S. Edwards, S. Hill, S. Bhaduri, N. Aliaga-Alcade, E. Bolin, S. Maccagnano, G. Christou, and D. N. Hendrickson (unpublished).

15. K. Park, M. A. Novotny, N. S. Dalal, S. Hill, and P. A. Rikvold, Phys. Rev. B **65**, 014426 (2002).

16. S. Hill, S. Maccagnano, K. Park, R. M. Achey, J. M. North, and N. S. Dalal, Phys. Rev. B **65**, 224410 (2002).

17. K. Blum, *Density Matrix Theory and Applications*, 2nd edition (Plenum, New York, 1996).

18. E. M. Chudnovsky and D. A. Garanin, Phys. Rev. Lett. **87**, 187203 (2001); Phys. Rev. B **65**, 094423 (2002).

19. A. Cornia, R. Sessoli, L. Sorace, D. Gatteschi, A. L. Barra, and C. Daiguebonne, Phys. Rev. Lett. **89**, 257201 (2002).

20. K. Park, M. A. Novotny, N. S. Dalal, S. Hill, and P. A. Rikvold, Phys. Rev. B **66**, 144409 (2002).

21. M. McMillan and W. Opechowski, Can. J. Phys. **38**, 1168 (1960); ibid. **39**, 1369 (1961).

22. J. H. Van Vleck, Phys. Rev. **74**, 1168 (1948).

23. M. N. Leuenberger and D. Loss, Phys. Rev. B **61**, 1286 (2000); ibid., **61**, 12200 (2000).

24. B. Parks, J. Loomis, E. Rumberger, D. Hendrickson, and G. Christou, Phys. Rev. B **64**, 184426 (2001).

25. A. Mukhin, B. Gorshunov, M. Dressel, C. Sangregorio, and D. Gatteschi, Phys. Rev. B **63**, 214411 (2001).

26. W. Wernsdorfer, N. Aliaga-Alcalde, D. N. Hendrickson, and G. Christou, Nature **416**, 406 (2002).

27. W. Wernsdorfer, S. Bhaduri, R. Tiron, D. N. Hendrickson, and G. Christou, Phys. Rev. Lett. **89**, 197201 (2002).

28. W. Wernsdorfer, S. Bhaduri, C. Boskovic, G. Christou, and D. N. Hendrickson, Phys. Rev. B **65**, 180403(R) (2002).

29. A. Abragam and B. Bleaney, *Electron Paramagnetic Resonance of Transition Ions* (Clarendon, Oxford, 1970).